The evolution of the localized interface optical-phonon modes in a finite superlattice with a structural defect

INSTITUTE OF PHYSICS PUBLISHING SEMICONDUCTOR SCIENCE AND TECHNOLOGY

Semicond. Sci. Technol. **20** (2005) 1027–1033 doi:10.1088/0268-1242/20/10/008

The evolution of the localized interface optical-phonon modes in a finite superlattice with a structural defect

Xin-Jun Wang[1], Lingling Wang[1], Wei-Qing Huang[1,2], Ke-Qiu Chen[1,2,3], Z Shuai[2] and B S Zou[1]

[1] Department of Applied Physics, Hunan University, Changsha 410082, People's Republic of China

[2] Laboratory of Organic Solids, Centre for Molecular Sciences, Institute of Chemistry, Chinese Academy of Sciences, 100080 Beijing, People's Republic of China

E-mail: keqiuchen@iccas.ac.cn or keqiuchen@hnu.cn and zgshuai@iccas.ac.cn

Received 4 July 2005, in final form 8 August 2005
Published 2 September 2005
Online at stacks.iop.org/SST/20/1027

Abstract

Using a transfer matrix method, we study the property of the interface optical-phonon modes (IOPMs) in a finite semiconductor superlattice (SL) with a structural defect layer in the dielectric continuum approximation. The results show that in such a structure there exist two types of localized IOPMs. They may appear either in the minigap or below and above the bulk bands, and their macroscopic electrostatic potentials are located in the vicinity of the defect layer or surface layer. The evolution of the modes localized in the vicinity of a different interface can clearly be tracked. In some cases, the degeneracy between localized IOPMs may occur, but the conservation of the total number of IOPMs is always kept for every value of the transversal wave number.

1. Introduction

Superlattices (SLs) with structural defects have attracted much attention due to the novel physical properties found in these kinds of structures in comparison with perfect SLs. Early in 1981, Combescot and Benoit a la Guillaume [1] studied the electron–hole state in SL with one or two structural defects. Since then, many researchers [2–6] explored the behaviours and properties of electron bound states in various SLs with structural defects both theoretically and experimentally. The vibrational properties in such types of structures have also been investigated extensively. The properties of the localized acoustic modes have been reported in various structures such as infinite SL with a structural defect layer [7–9], semi-infinite SL with a substrate or an adsorbed layer [10] and in finite SL [11–15]. Since the interface optical-phonon modes (IOPMs) were found to play a dominant role in electron–phonon interactions in quantum wells and SLs [16–21], the properties of the localized and extended IOPMs have been a very interesting subject in SL with the presence of inhomogeneities such as surface, interface or defect layer. The interface optical phonons in an infinite superlattice [22] and in a finite multilayer structure [23] were derived. The surface phonon polaritons in a two-layer semi-infinite superlattice were studied by Bah *et al* [24]. The dispersion curves of surface phonons in a finite superlattice were ascertained [25–27]. The dependence of surface modes on the outermost layer in semi-infinite and finite SLs have also been analysed by Streight and Mills [28] and Tsuruoka *et al* [29], respectively.

Recently, Chen *et al* investigated the localized IOPMs in coupled semi-infinite SL with structural defect layers [30] and in a semi-infinite SL with a cap layer [31]. Their works show that for the infinite SL with defect layers the localized IOPMs always appear in pairs inside the minigap and possess either symmetric or antisymmetric behaviours with respect to the centre of the defect layer, corresponding to longitudinal and transverse vibrations, respectively; while for the semi-infinite SL, the surface modes may exist inside the minigap, above or below the bulk band. It is known from these studies that the formation of the bulk bands in SL results from the periodicity coupling between two adjacent dielectric layers, while the localized IOPMs originate from

[3] Author to whom any correspondence should be addressed.

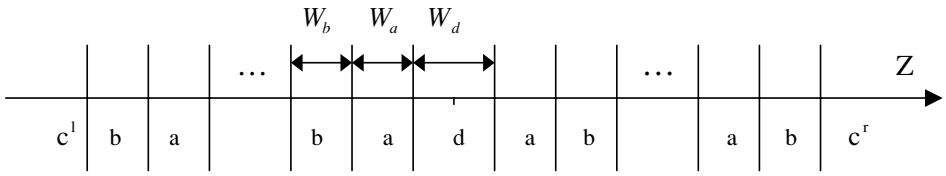

Figure 1. A schematic diagram of two semi-finite SLs with an embedded structural defect layer d. W_a, W_b and W_d denote, respectively, the thickness of constituent layers of the unit cell of the SL and defect layer. The centre of the defect layer is taken as the coordinate origin ($z = 0$).

the periodicity-broken coupling due to the existence of the inhomogeneous layers such as surface, interface or defect layer. The periodicity-broken coupling leads to the appearance of new splitting levels. Some of them may lie within the bulk bands and develop into the delocalized scattering modes, and the others reside in the minigaps or below and above the bulk bands, and become localized modes. However, they cannot track the delocalized scattering modes due to their works focused on the infinite or semi-infinite SLs where these modes merge into the bulk bands. To observe clearly the evolution of the splitting levels due to periodicity-broken coupling from the localized modes lying in the minigaps to the delocalized scattering modes (extended modes) in the bulk bands, the present paper investigates IOPMs in a finite SL with a structural defect. Note that the discrete characteristics of the IOPMs in the finite SL enable one to see clearly the evolution of all the IOPMs with structural parameters or transversal wave number.

This paper is organized as follows. In section 2, we present a brief description of the model and necessary formulae used in calculations. The calculated results are given with analyses in section 3. Finally, in section 4, a summary is made.

2. Model and formalism

In fact, the number of the periodicity of the SL is finite in a real system, which is grown on a substrate and usually has a cap layer (sometimes serves as a phonon detector layer). Here, we consider a structure as shown in figure 1, in which a defect layer labelled as d (material AlAs) with a thickness of W_d is sandwiched between two finite coupled SLs with a cell unit composed of a (GaAs) and b (AlAs) materials, and the substrates are frequency-dependent uniform dielectric medium (GaAs) labelled as c^l and c^r, respectively. The dielectric constants of materials a, b, c^l, c^r and d are $\epsilon_a(\omega)$, $\epsilon_b(\omega)$, $\epsilon_c^l(\omega)$, $\epsilon_c^r(\omega)$ and $\epsilon_d(\omega)$, respectively. W_a, W_b and W_d denote the thickness of constituent layers a, b and defect layer d, respectively. The number of the period at each side of the defect layer is n. The period is $W = W_a + W_b$.

In the present paper, we introduce the transfer matrix method to investigate the localized IOPMs in the dielectric continuum model. The dielectric continuum model for spatially confined systems was first developed by Fuchs and Kliewer [32]. Strictly speaking, the dielectric continuum model is valid in the long-wavelength limit in bulk material. However, this model is a rather good approximation in several mini-Brillouin-zone (MBZ) scales of wave number q for the SL structure due to the period of the SL being much larger than the lattice constant of the bulk materials. This conclusion has been confirmed by microscopic calculations [17] and Raman experiments [33]. Regardless of retardation in treatment of IOPMs, the macroscopic electrostatic potential $\phi(r)$ must obey Laplace's equation

$$\nabla^2\phi(r) = 0. \tag{1}$$

As we have translational invariance in the two directions (x, y) parallel to the interface, and thus each material is assumed isotropic, the electrostatic potential can be noted by $\phi(r) = \phi(z)\,e^{iq_\parallel y}$, where $q_\parallel$ is the component lying on the (x, y) plane of the propagation vector in the superlattice $\vec{q} = (q_\parallel, q_z)$ and is the same for each material in the structure. For simplicity, we call $q_\parallel$ the transverse wave number. Then, we can write down the electrostatic potential in each slab as follows:

$$\phi(z) = c^l \exp(q_\parallel(z + W_d/2 + nW)) \quad z \leqslant -(W_d/2 + nW), \tag{2}$$

$$\phi(z) = B^l_{n,1}\exp(q_\parallel[z + W_d/2 + (n-1)W + W_a]) + B^l_{n,2}\exp(-q_\parallel[z + W_d/2 + (n-1)W + W_a]) \quad -(W_d/2 + nW) \leqslant z \leqslant -[W_d/2 + W_a + (n-1)W], \tag{3}$$

$$\phi(z) = A^l_{n,1}\exp(q_\parallel[z + W_d/2 + (n-1)W]) + A^l_{n,2}\exp(-q_\parallel[z + W_d/2 + (n-1)W]) \quad -[W_d/2 + (n-1)W + W_a] \leqslant z \leqslant -[W_d/2 + (n-1)W], \quad \ldots \tag{4}$$

$$\phi(z) = D_1\exp(q_\parallel z) + D_2\exp(-q_\parallel z) \quad -(W_d/2) \leqslant z \leqslant W_d/2, \quad \ldots \tag{5}$$

$$\phi(z) = A^r_{n,1}\exp(q_\parallel[z - W_d/2 - (n-1)W]) + A^r_{n,2} \times \exp(-q_\parallel[z - W_d/2 - (n-1)W]) \quad W_d/2 + (n-1)W \leqslant z \leqslant W_d/2 + (n-1)W + W_a, \tag{6}$$

$$\phi(z) = B^r_{n,1}\exp(q_\parallel[z - W_d/2 - (n-1)W - W_a]) + B^r_{n,2}\exp(-q_\parallel[z - W_d/2 - (n-1)W - W_a]) \quad W_d/2 + (n-1)W + W_a \leqslant z \leqslant W_d/2 + nW, \tag{7}$$

$$\phi(z) = c^r\exp(-q_\parallel(z - W_d/2 - nW)) \quad z \geqslant W_d/2 + nW. \tag{8}$$

In the dielectric continuum model, the electrostatic boundary conditions are employed to interrelate various coefficients appearing in the above-mentioned expressions: the electrostatic potential ϕ and the normal component of the displacement field ($D = \epsilon E$) should be continuous at

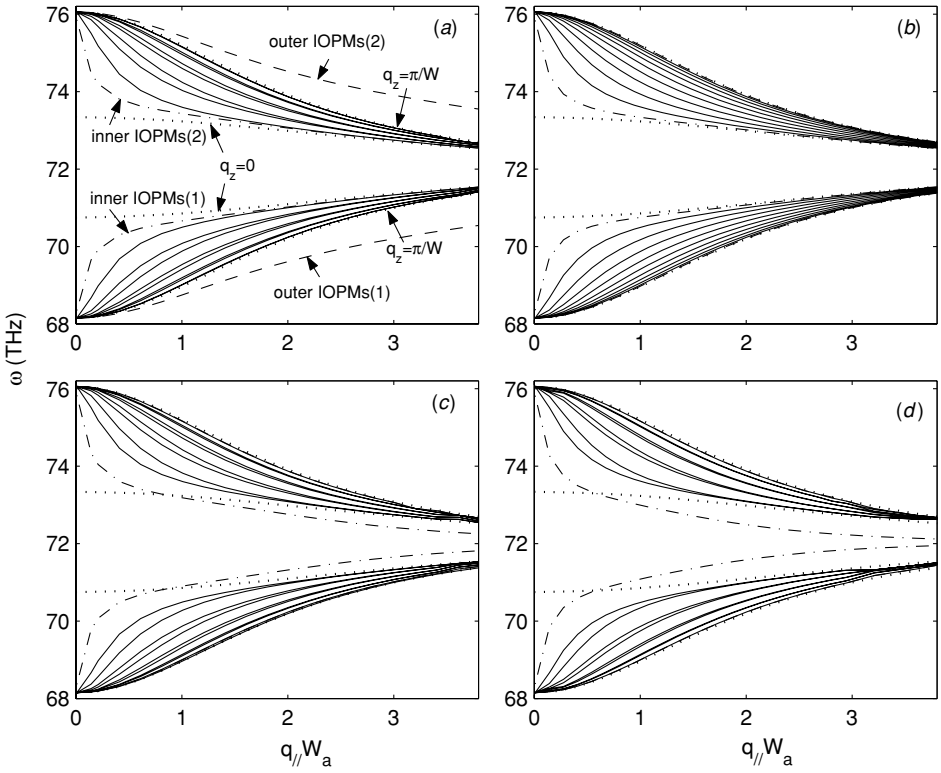

Figure 2. The calculated frequencies of the AlAs-like IOPMs as a function of the transversal wave number $q_\parallel$ for different thicknesses of defect layer. (a)–(d) correspond to $W_d = 5$, 10, 15 and 20 nm, respectively. The dashed curves labelled as outer IOPMs(1), and outer IOPMs(2) represent the IOPMs lying below the lower band and above the upper band, respectively; the dot-dashed curves labelled as inner IOPMs(1) and inner IOPMs(2) represent the lowest IOPM of the upper band and the highest IOPM of the lower band, respectively; and the solid curves indicate the rest IOPMs for the finite superlattice. Four dotted curves represent the limits, which correspond to the centre and edge of the mini-Brillouin zone (i.e., $q_z = 0$ and $q_z = \pi/W$), respectively, of the continuous bands for the infinite superlattice with the same constituent configurations. Here, we take $W_a = 20$ nm, $W_b = 10$ nm. The number of the period at each side of the defect layer is $n = 5$.

each interface. Here, it should be noted in particular that by using the continuum theory with both electrostatic and mechanical boundary conditions being fulfilled, Chamberlain *et al* [34] and Klimin *et al* [35] investigated interface optical-phonon spectra in the superlattice and multilayer structure, respectively. However, their calculated results for the interface optical-phonon modes also show that the dielectric continuum model may be considered as a quite correct first approximation of continuum theory when the slab thicknesses are much larger than the lattice constants. Then we can derive the following equation:

$$\begin{pmatrix} c^l \\ q_\parallel \epsilon_c^l c^l \end{pmatrix} = T \begin{pmatrix} 0 \\ c^r \end{pmatrix}, \tag{9}$$

where

$$T = T(W_b, \epsilon_b) T_l^{(n-1)} M^{-1}(\epsilon_b) T(W_a, \epsilon_a) T_{ad} \times T_{da} T^{-1}(-W_a, \epsilon_a) M(\epsilon_b) T_r^{(n-1)} T^{-1}(-W_b, \epsilon_b) C_0, \tag{10}$$

with

$$T(z, \epsilon) = \begin{pmatrix} \mathrm{e}^{-q_\parallel z} & \mathrm{e}^{q_\parallel z} \\ q_\parallel \epsilon \mathrm{e}^{-q_\parallel z} & -q_\parallel \epsilon \mathrm{e}^{q_\parallel z} \end{pmatrix}, \tag{11}$$

$$M(\epsilon) = \begin{pmatrix} 1 & 1 \\ q_\parallel \epsilon & -q_\parallel \epsilon \end{pmatrix}, \tag{12}$$

$$T_l = M^{-1}(\epsilon_b) T(W_a, \epsilon_a) M^{-1}(\epsilon_a) T(W_b, \epsilon_b), \tag{13}$$

$$T_r = T^{-1}(-W_b, \epsilon_b) M(\epsilon_a) T^{-1}(-W_a, \epsilon_a) M(\epsilon_b), \tag{14}$$

$$T_{ad} = M^{-1}(\epsilon_a) T(W_d/2, \epsilon_d), \tag{15}$$

$$T_{da} = T^{-1}(-W_d/2, \epsilon_d) M(\epsilon_a), \tag{16}$$

$$C_0 = \begin{pmatrix} 0 & 1 \\ 0 & -q_\parallel \epsilon_c^r \end{pmatrix}. \tag{17}$$

By combining equations (9)–(17) , the implicit dispersion relation for the structure shown in figure 1 is obtained:

$$T_{22} - q_\parallel \epsilon_c^l T_{12} = 0, \tag{18}$$

where T_{12} and T_{22} are the elements of matrix T. For the binary crystal AlAs or GaAs, the dielectric function has the form

$$\epsilon_i(\omega) = \epsilon_{\infty i} \frac{(\omega^2 - \omega_{LOi}^2)}{(\omega^2 - \omega_{TOi}^2)}, \qquad (i = a, b) \tag{19}$$

where i corresponds to GaAs (a) or AlAs (b), ϵ_∞ is optical dielectric constant, ω_{LOi} (ω_{TOi}) is the longitudinal (transverse) optical-phonon frequency of corresponding material. In the calculations, we employ those values of dielectric constants and phonon frequencies of GaAs and AlAs referred to [36, 37]: $\epsilon_\infty(\mathrm{GaAs}) = 10.89$, $\epsilon_\infty(\mathrm{AlAs}) = 8.16$, $\omega_{LO}(\mathrm{GaAs}) = 55.045$, $\omega_{TO}(\mathrm{GaAs}) = 50.550$, $\omega_{LO}(\mathrm{AlAs}) = 76.061$, $\omega_{TO}(\mathrm{AlAs}) = 68.150$ Thz.

3. Numerical results and discussion

First, in figure 2, we show the dispersion curves of the AlAs-like IOPMs for different thicknesses of defect layer d: (a)–(d)

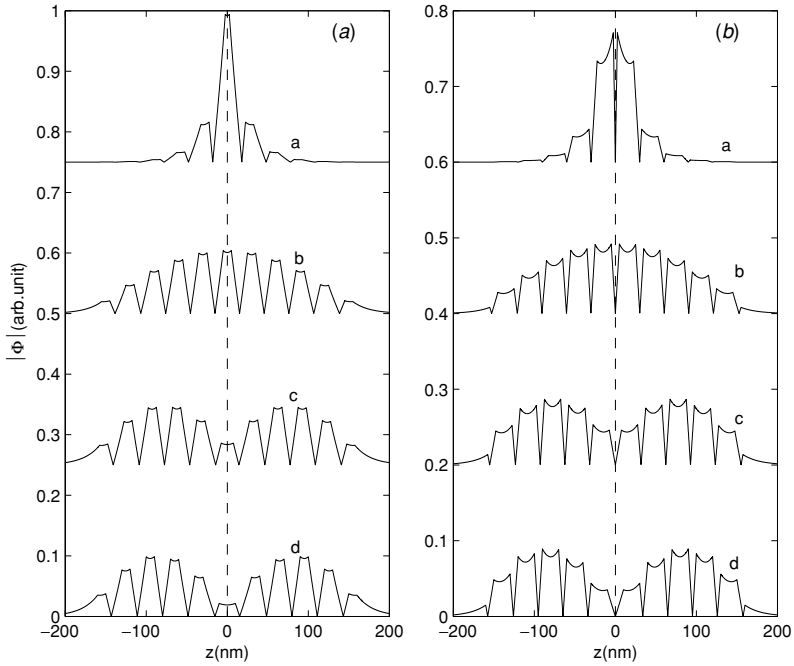

Figure 3. Modulus of the electrostatic potentials $|\phi(z)|$: curves a–d in figures (a) and (b) correspond to $|\phi(z)|$ of the outer IOPMs(1) and IOPMs(2) for $W_d = 5$, 10, 15 and 20 nm in figure 2 with $q_\parallel W_a = 1$, respectively. The vertical dashed lines represent $z = 0$. For clarity, two consecutive curves in (a) and (b) have been vertically separated by 0.25 and 0.20, respectively.

correspond to $W_d = 5$, 10, 15 and 20 nm, respectively. Here, we take $n = 5$, $W_a = 20$ nm, $W_b = 10$ nm. To show clearly the relation between the localization characteristics of the interface modes and their locations falling inside or outside the bands,the limits, which correspond to the centre and edge of the mini-Brillouin zone (i.e. $q_z = 0$ and $q_z = \pi/W$), respectively, of the continuous bands for the infinite superlattice with the same constituent configurations are also depicted. Note that the continuous bands in the infinite and semi-infinite SLs will break up into the discrete modes in the finite SL, so we can clearly observe the total number for every value of transverse wave number in the finite SL. For the structure with $n = 5$, there exist 22 allowed discrete AlAs-like modes, which fall into two symmetric bands separated by a minigap. The minigap gradually narrows with the increase of the transverse wave number $q_\parallel$, forming a high density of states for large $q_\parallel$. From figure 2, it is found that the boundaries of the band in the structure considered here are very close to the values found in the infinite superlattice except in the region $q_\parallel \approx 0$. This results from the fact that the penetration depth of the phonon amplitude is typically few periods, but more periods need to be taken into account for interface phonon modes near the zone centre due to their long wavelength. Why only five periods at each side of the defect layer are considered here is because when more periods are involved, the localized modes and surface modes discussed below do not vary in characteristics, while it is difficult to take count of the number of the total IOPMs. In order to observe the localization degree of the IOPMs, in figures 3 and 4, we map out the moduli of the electrostatic potential $|\phi(z)|$: figures 3(a) and (b) correspond to the outer IOPMs(1) and IOPMs(2), while figures 4(a) and (b) to the inner IOPMs(1) and IOPMs(2) in figure 2 with $q_\parallel W_a = 1$, respectively.

From figures 2(a) and 3, for $W_d = 5$ nm, it is clearly seen that both the outer-IOPM(1) and outer-IOPM(2) lying outside the band (extended modes) are strongly localized in the vicinity of the defect layer with even and odd parities, respectively. We call these IOPMs localized modes. With the increase of the thickness of the defect layer, the localized modes shift towards the band edges and the localized degree gradually weakens. As W_d is equal to 10 nm, namely the structure is recovered to perfect finite SL, the localized modes (see figure 2(b)) merge into the band and their electrostatic potentials are similar to those of the extended modes in characteristics. With any further increase of W_d, the outer-IOPMs remain in the extended modes. From figures 2 and 4, we can also find that, with the increase of the thickness of the defect layer, both the inner-IOPM(1) and inner-IOPM(2) with even and odd parities, respectively, gradually extract from the band and shift towards the centre frequency of the minigap. Their evolution from the extended modes to the localized modes can clearly be seen from figure 4. Moreover, we calculate the moduli of the macroscopic electrostatic potentials for the rest modes; it is found that these modes mainly localize in the constituent layers of the finite SL, and are called the extended modes. We find from our calculations that the macroscopic electrostatic potentials for all IOPMs alternate between even and odd parities; this may be attributed to the fact that the structure considered here is symmetric about the midplane of the defect layer and so each eigenstate in the confined system with space-reverse symmetry has a definite parity as long as the eigenstate is non-degenerated. Note that all the peaks and valleys in all the moduli of the macroscopic electrostatic potentials are located at the interfaces and the bisectors of slabs, respectively, which is similar to the results presented in [30].

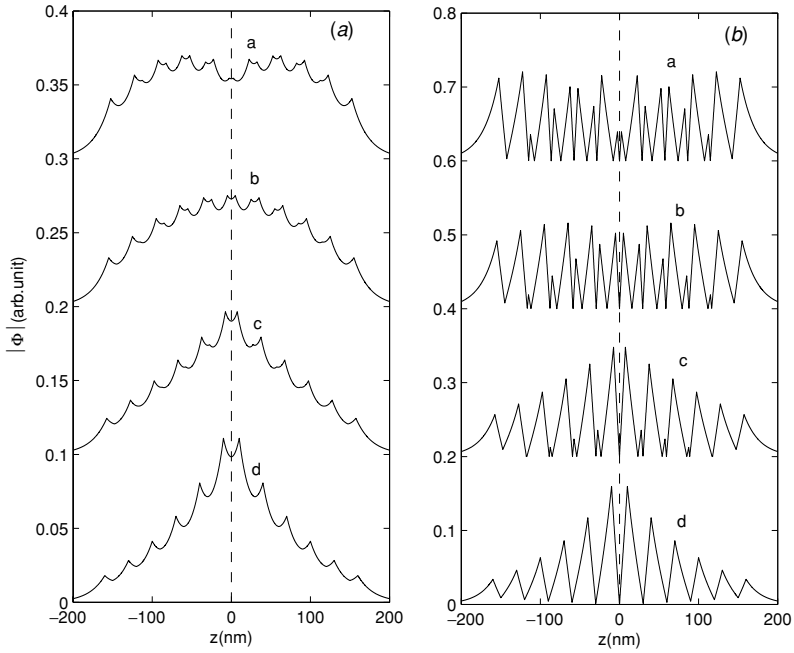

Figure 4. Moduli of the electrostatic potentials $|\phi(z)|$ correspond to the inner IOPMs(1) and IOPMs(2) in figure 2 with $q_{\parallel}W_a = 1$, respectively. For clarity, two consecutive curves in (a) and (b) have been vertically separated by 0.10 and 0.20, respectively. Explanations for all curves are the same as in figure 3.

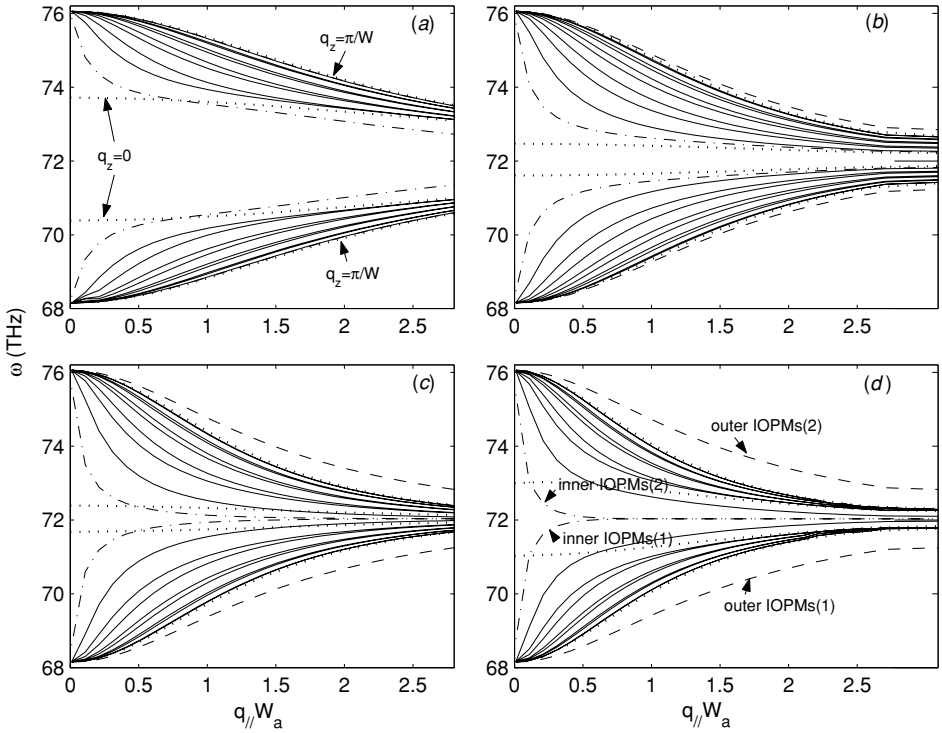

Figure 5. The calculated frequencies of the AlAs-like IOPMs as a function of the transversal wave number $q_{\parallel}$ for different widths of constituent layer b. (a)–(d) correspond to $W_b = 4$, 8, 12 and 17 nm. Here, W_a, W_d and n are taken as 10 nm, 6 nm and 5, respectively. Explanations for all curves are the same as in figure 2.

The dispersion curves of the AlAs-like IOPMs for different W_b are shown in figures 5(a)–(d) correspond to $W_b =$ 4, 8, 12 and 17 nm, respectively. Here, W_a, W_d and n are taken as 10 nm, 6 nm and 5, respectively. Figures 6 and 7 describe the moduli of the electrostatic potentials $|\phi(z)|$ corresponding to the outer IOPM(1) and IOPM(2), and the inner IOPM(1) and IOPM(2) in figure 5 with $q_{\parallel}W_a = 1$, respectively. From these figures, it is clearly seen that the outer IOPM(1) and IOPM(2) first lie in the bands, and that their wavefunctions are mainly located in the constituent layers. When increasing W_b, the outer IOPM(1) and IOPM(2) shift far from the extended modes and develop into localized modes, their wavefunctions mainly

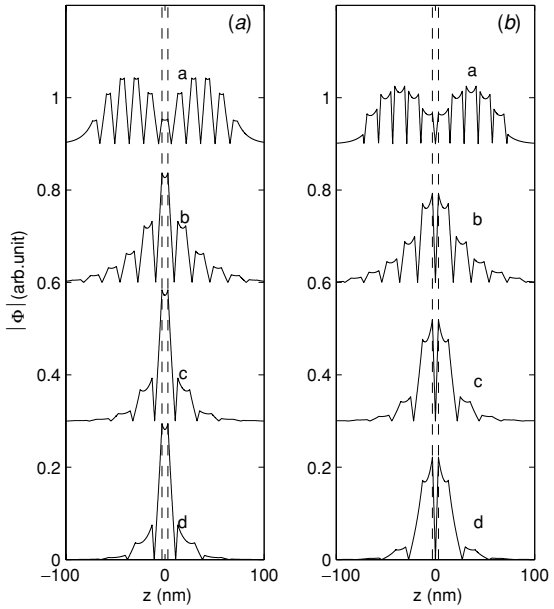

Figure 6. Modulus of the electrostatic potentials $|\phi(z)|$: curves a–d in figures (*a*) and (*b*) correspond to $|\phi(z)|$ of the outer IOPMs(1) and IOPMs(2) for $W_b = 4$, 8, 12 and 17 nm in figure 5 with $q_\parallel W_a = 1$, respectively. The vertical dashed line corresponds to the edge of the defect layer. For clarity, two consecutive curves in (*a*) and (*b*) have been vertically separated by 0.3.

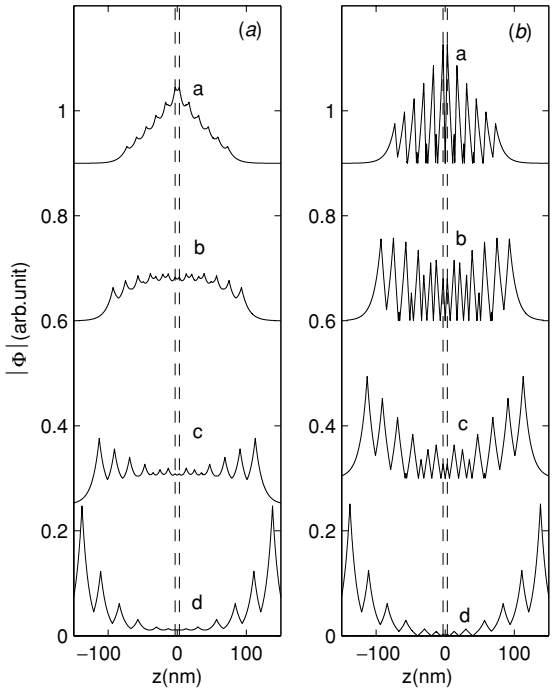

Figure 7. Moduli of the electrostatic potentials $|\phi(z)|$ correspond to the inner IOPMs(1) and IOPMs(2) in figure 5 with $q_\parallel W_a = 1$, respectively. For clarity, two consecutive curves in (*a*) and (*b*) have been vertically separated by 0.25 and 0.30, respectively. Explanations for all curves are the same as in figure 6.

localize in the vicinity of the defect layer. With the further increase of W_b, the localization degree of the outer IOPM(1) and IOPM(2) in the vicinity of the defect layer becomes higher. However, for the inner IOPM(1) and IOPM(2) when $W_b < W_a$, they shift towards the band in spite of the minigap becoming small, and these IOPMs in characteristics change from localized modes to the extended modes. When $W_b > W_a$, both the inner IOPM(1) and IOPM(2) develop in characteristics into two surface modes. And the localization degree of these surface modes at their corresponding surfaces become stronger as W_b is increased (see curves c, d in figures 7(*a*) and (*b*)). Here, it should be noted in particular that in such a structure, interface optical-phonon modes are divided into extended modes, localized modes and surface modes according to their macroscopic electrostatic potentials being mainly localized in the vicinity of constituent layers, defect layer, or surface in the superlattice. When increasing the number of layers in the superlattice, the discrete extended modes gradually come into bands, and the localized modes and the surface modes lie in the minigap above or below the band. The existence and features of the localized modes and surface modes result from the periodicity-broken coupling due to the existence of the inhomogeneous layers such as defect layers or surfaces. From figure 5(*d*), it is clearly seen that with the increase of transverse wave number the inner IOPM(1) and IOPM(2) gradually approach each other and finally only one branch of inner IOPM can be seen in the gap. This behaviour appears somewhat suspicious in view of the conservation of the total number of the IOPMs for every value of the transversal wave number $q_\parallel$. However, from the evolution of the macroscopic electrostatic potentials of these IOPMs, it can be inferred that though both the inner IOPM(1) and IOPM(2) are of the same frequency, they have different parity. One of them is symmetric, while the other is antisymmetric with respect to the centre of the defect layer. So the conservation of the total number of the IOPMs is still kept. According to the evolution of the macroscopic electrostatic potentials of these IOPMs, we can also infer that when W_b is large enough the degeneracy will occur between both the inner IOPM(1) and IOPM(2) for the whole range of the transversal wave number explored here. When W_b is increased, the thickness of the SL also increases, the interaction will weaken between the surface excitation localized at the left surface and that at the right surface in such structure. So the splitting wavelength occurs at a larger value. Moreover, it is found that when $W_b > W_a$, two branches of interface optical phonon modes next to the inner IOPM(1) and IOPM(2), respectively, fall inside the minigap, and the calculations show that their localization characteristics are similar to the localized modes.

These phenomena can be understood from a physical point of view. For a finite SL with a structural defect layer, the periodic coupling is locally broken down around both the surfaces and defect layer. New coupling among them arises. This periodicity-broken coupling will lead to the appearance of new splitting levels. They reside in the gaps or below and above the bulk bands, and develop into localized modes or surface modes. Their macroscopic electrostatic potentials are mainly located in the vicinity of the defect layers or surfaces. The existence and the characteristics of the localized IOPMs depend on the coupling strength. And the coupling strength depends on dielectric response characteristics ϵ_ω (namely, the nature of the material) of the constituent layers, the relative thickness and the stack sequence of the SLs, especially the nature and thickness of the defect layers as intermediate.

So, for different structural parameters, different localization characteristics are found. Here, it is worth, in particular, pointing out that for the structure considered here, the localized IOPMs exist not only in the minigap but also below and above the bulk bands, while for the structure presented in [30], the localized IOPMs exist only in the minigap. This should be attributed to the different couplings in different structures. Because the structure considered here is symmetric about the midplane of the defect layer, therefore, the localized IOPMs always appear in pairs (odd–even parity pair). These results tell us that the spectra of the localized IOPMs can be engineered by adjusting structural parameters.

For GaAs-like localized IOPMs, similar phenomena can be observed except that the symmetries of the macroscopic electrostatic potentials $\phi(z)$ are just reversed.

4. Summary

In this paper, we have presented the properties of the interface optical-phonon modes in a finite superlattice with a structural defect. In the present system, there exist two types of localized modes. Their macroscopic electrostatic potentials are mainly located in the vicinity of the defect layer or surface layer, respectively. The calculated results show that the existence and characteristics of the localized IOPMs depend on the nature of the material of the constituent layers, the relative thickness and the stack sequence of the SLs, especially the nature and thickness of the defect layers as intermediate. In some cases, the dispersion curves of some localized IOPMs are joined together. This looks as if the total number of the IOPMs is different for different transverse wave vectors. Our results show that this behaviour results from the degeneracy between the localized IOPMs. Though they are of the same frequency, their macroscopic electrostatic potentials are different. So the number of the total IOPMs including both the delocalized scattering modes and localized modes is kept for every value of the wave vector $q_{\parallel}$.

Acknowledgments

This work was supported by the National Natural Science Foundation of China (project no. 90403026) and the Chinese Academy of Sciences.

References

[1] Combescot M and Benoit a la Guillaume C 1981 *Solid State Commun.* **39** 651
[2] Ihm G, Noh S K, Falk M L and Lim K Y 1992 *J. Appl. Phys.* **72** 5325
[3] Suris R A and Lavallard P 1994 *Phys. Rev.* B **50** 8875
[4] Indjin D, Milanovic V and Ikonic Z 1997 *Phys. Rev.* B **55** 9722
[5] Wang X H, Gu B Y, Yang G Z and Wang J 1998 *Phys. Rev.* B **58** 4629
[6] Huang W-Q, Chen K-Q, Shuai Z, Wang L and Hu W 2004 *Phys. Lett.* A **325** 70
[7] Chen K-Q, Wang X-H and Gu B-Y 2000 *Phys. Rev.* B **61** 12075
[8] Wang X-H, Chen K-Q and Gu B-Y 2002 *J. Appl. Phys.* **92** 5113
[9] Mizuno S 2002 *Phys. Rev.* B **65** 193302
[10] Bria D, El Boudouti E H, Nougaoui A, Djafari-Rouhani B and Velasco V R 1999 *Phys. Rev.* B **60** 2505
Bria D, El Boudouti E H, Nougaoui A, Djafari-Rouhani B and Velasco V R 2000 *Phys. Rev.* B **61** 15858
[11] Mizuno S and Tamura S I 1992 *Phys. Rev.* B **45** 13423
Mizuno S and Tamura S I 1996 *Phys. Rev.* B **53** 4549
[12] James R, Woodley S M, Dyer C M and Humphrey V F 1995 *J. Acoust. Soc. Am.* **97** 2041
[13] Hammouchi M, El Boudouti E H, Nougaoui A, Djafari-Rouhani B, Lahlaouti M L H, Akjouj A and Dobrzynski L 1999 *Phys. Rev.* B **59** 1999
[14] Mizoguchi K, Takeuchi H, Hino T and Nakayama M 2002 *J. Phys.: Condens. Matter* **14** 103
[15] Pu N-W and Bokor J 2003 *Phys. Rev. Lett.* **91** 076101
[16] Zucker J E, Pinczuk A, Chemla D S, Gossard A and Wiegmann W 1984 *Phys. Rev. Lett.* **53** 1280
[17] Huang K and Zhu B F 1988 *Phys. Rev.* B **38** 2183
Huang K and Zhu B F 1988 *Phys. Rev.* B **38** 13377
[18] Mori N and Ando T 1989 *Phys. Rev.* B **40** 6175
[19] Duan W, Zhu J-L and Gu B-L 1994 *Phys. Rev.* B **49** 14403
[20] Zheng R and Matsuura M 1999 *Phys. Rev.* B **60** 4937
[21] Kim D K, Roblin P, Soh K-S and Kim C K 2002 *Phys. Rev.* B **65** 115328
[22] Pokatilov E P and Beril S I 1982 *Phys. Status Solidi* b **110** K75
[23] Fomin V M and Pokatilov E P 1985 *Phys. Status Solidi* b **132** 69
[24] Bah M L, Akjouj A, El Boudouti E H, Djafari-Rouhani B and Dobrzynski L 1995 *J. Phys.: Condens. Matter* **7** 3445
[25] Johnson B L, Weiler J T and Camley R E 1985 *Phys. Rev.* B **32** 6544
[26] Nkoma J S 1987 *Surf. Sci.* **191** 5951
[27] Liu W-M, Eliasson G and Quinn J J 1985 *Solid State Commun.* **55** 533
[28] Streight S R and Mills D L 1987 *Phys. Rev.* B **35** 6337
[29] Tsuruoka T, Uehara Y and Ushioda S 1994 *Phys. Rev.* B **49** 4745
[30] Chen K-Q, Wang X-H and Gu B-Y 2000 *Phys. Rev.* B **62** 9919
[31] Chen K-Q, Duan W, Wu J, Gu B-L and Gu B-Y 2002 *J. Phys.: Condens. Matter* **14** 13761
[32] Fuchs R and Kliewer K L 1965 *Phys. Rev.* **140** A2076
[33] Sood A K, Menendez J, Cardona M and Ploog K 1985 *Phys. Rev. Lett.* **54** 2115
[34] Chamberlain M P, Cardona M and Ridley B K 1993 *Phys. Rev.* B **48** 14356
[35] Klimin S N, Pokatilov E P and Fomin V M 1995 *Phys. Status Soldi* b **190** 441
[36] Yu S G, Kim K W, Stroscio M A, Iafrate G J, Sun J-P and Haddad G I 1997 *J. Appl. Phys.* **82** 3363
[37] Adachi S 1985 *J. Appl. Phys.* **58** R1